Materials Research. 2016; 19(3): 673-679
DOI:http://dx.doi.org/10.1590/1980-5373-MR-2016-0009

Novel Ag_3PO_4/CeO_2 p-n Hierarchical Heterojunction with Enhanced Photocatalytic Performance

Wei Zhang[a]*, Chao Hu[a], Wei Zhai[a], Zhengluo Wang[a], Yaxin Sun[a], Fangli Chi[a], Songlin Ran[a], Xianguo Liu[a], Yaohui Lv[a]*

[a]School of Materials Science and Engineering, Anhui Key Laboratory of Metal Materials and Processing, Anhui University of Technology, Anhui, Maanshan, 243002, P. R. China.

Received: January 7, 2016; Revised: March 10, 2016; Accepted: April 4, 2016

The composite Ag_3PO_4/CeO_2 photocatlyst, a novel p-n type heterojunction, has been successfully fabricated through a facile hydrothermal process combined with a successive *in situ* precipitation technique. The X-ray diffraction (XRD), scanning electron microscopy (SEM), high-resolution transmission electron microscopy (HRTEM) and UV-visible diffuse reflectance spectra (DRS) were used to characterize the as-obtained products. The SEM and TEM image show that CeO_2 particles have been successfully loaded and well distributed in the surface of Ag_3PO_4. The photocatalytic activities of the p-Ag_3PO_4/n-CeO_2 heterojunctions were investigated for their efficiency on the degradation of Rhodamine B (RhB) under ultra-violet light and visible light irradiation, and the results showed that the p-Ag_3PO_4/n-CeO_2 heterojunctions possessed remarkable photocatalytic activities. The enhanced photocatalytic activity can be attributed to the extended absorption in the visible light region resulting from the Ag_3PO_4 and the effective separation of photogenerated carriers driven by the internal electrostatic field in the junction region.

Keywords: *P-n junction, Semiconductors, Photocatalytic activity*

1. Introduction

As a result of an imminent energy crisis and growing pollution issues, many researchers are aiming at the utilization of renewable energy sources such as wind or solar light[1]. Among all the approaches for renewable energy utilization, one of the most remarkable one is the use of solar energy for photocatalytic degradation of organic pollutants and for hydrogen generation via water splitting[2]. However, some traditional photocatalysts such as TiO_2, ZnO, NiO can absorb only ultraviolet light due to their wide band gaps. Thus, the development of visible-light-driven (VLD) photocatalysts has attracted increasing attention in order to efficiency utilize solar light in the visible region (700 nm > λ >400 nm). Recently, Ye and co-workers reported that Ag_3PO_4 semiconductor exhibited a high-efficient usage of visible light (up to 90%) for O_2 evolution from water as well as effective photodecomposition of organic compounds[3-5]. Unfortunately, one major limitation of this novel photocatalyst is unstable upon photo-illumination, and it is easily corroded by the photogenerated electrons ($4Ag_3PO_4 + 6H_2O + 12h^+ + 12e^- \rightarrow 12Ag + 4H_3PO_4 + 3O_2$)[3]. Therefore, a key issue is how to enhance the stability of Ag_3PO_4 photocatalyst by improving the separation efficiency of the photogenerated electrons and holes.

It has been reported that coupling two or more semiconductors with appropriate band positions is an efficient strategy to effectively enhance the photocatalytic activities of the semiconductor photocatalysts, because it can improve the separation efficiency of photogenerated electron-hole pairs and solar light absorption ability[6, 7] . In particular, the fabrication of a p-n junction photocatalyst is believed to be very effective strategy to significantly enhance the photocatalytic activity of photocatalysts because of the existence of an internal electric field[8]. For instance, it has been reported that BiOI/SnS_2 heterojunction flowerlike structure demonstrate an enhanced visible-light photocatalytic activity due to the formation of the p-n junction between p-type BiOI and n-type SnS_2[9].

Cerium dioxide (CeO_2) is an n-type semiconductor with a wide energy band gap of 3.2 eV, indicating that CeO_2 can only respond to ultraviolet light. In addition, the photocatalytic properties of CeO_2 are predominantly restricted by the rapid recombination of photo-induced electrons and holes. Although a single CeO_2 material exhibits poor photocatalytic performance owing to its low charge-transfer rate, previous investigations indicated that CeO_2 is an excellent cocatalyst with other semiconductors such as Fe_2O_3, Bi_2O_3, CdS, g-C_3N_4, and so on[10-13], because of the improved charge separation and oxygen reduction at the interfaces between the two coupled catalysts. Ag_3PO_4 is a p-type semiconductor[3] with indirect and direct band gaps are 2.36 eV and 2.43 eV, respectively. On account of that the combination of CeO_2 and Ag_3PO_4 possess well matched overlapping band structure[14], p-n hetero-junctions could be fabricated by coupling CeO_2 with Ag_3PO_4, which will bring more effective interface transfer of photo-generated electrons and holes to restrain the recombination. Besides, owe to its narrower band gap relative to CeO_2, Ag_3PO_4 is able to act as

*e-mail: yaohui@ahut.edu.cn; zw2010@ahut.edu.cn

effcient photosensitizer to enlarge the light response range under solar light irradiation.

In this paper, we applied a facile process to successfully fabricate Ag_3PO_4/CeO_2 hetero-junctions by an *in situ* precipitation method. The as-prepared Ag_3PO_4/CeO_2 hetero-junctions demonstrated much higher activity than that of single Ag_3PO_4 or CeO_2 under the irradiation of visible light as well as UV light. Furthermore, the stability of the Ag_3PO_4/CeO_2 photocatalyst was investigated and a photocatalytic mechanism under visible-light irradiation was proposed.

2. Experimental section

2.1. Preparation of CeO_2 nano-particles

All reagents are of analytic grade and used without further purification. In a typical procedure, 1.0 g of cerium nitrate hexahydrate ($Ce(NO_3)_3 \cdot 6H_2O$) was fully dissolved in 40 mL formalin solution under vigorous magnetic stirring for 10 min. Afterwards, 1.5 g of sodium hydroxide (NaOH) was added into the above solution and was transferred in to a 50 mL capacity Teflon-lined stainless steel autoclave. Subsequently, the autoclave was laid in an oven at 140 °C for 40 h under autogenous pressure and static conditions. After reaction, the suspension was cooled down to room temperature. The as-obtained powder samples were centrifuged and washed with distilled water, and then dried completely in an oven at 80 °C for 12 h. The dried powders were heated to 450 °C in air at a rate of 5 °C min^{-1} and calcined for 5 h. The light yellow powders were obtained.

2.2. Preparation of Ag_3PO_4/CeO_2 heterostructure composite

The preparation of the Ag_3PO_4/CeO_2 heterostructure composite was carried out by an *in situ* precipitation method. In a typical synthesis process, 0.1 g of as-prepared CeO_2 nano-particles were dispersed in 150 mL deionized water and sonicated for 30 min. Immediately after sonication, $AgNO_3$ aqueous solution (100 mL, 0.012 mol L^{-1}) was added to the white CeO_2 dispersed solution, followed by magnetic stirring. Na_2HPO_4 aqueous solution (200 mL, 0.003 mol L^{-1}) was then added dropwise, accompanied with thorough stirring until the color of the solution changed from white to yellow. The precipitate was centrifuged and washed several times with deionized water and absolute ethanol, and dried at 80 °C for 10 h. For comparison, Ag_3PO_4 particles were also prepared under the same conditions without the presence of CeO_2 nanoparticles.

2.3. Characterization

X-ray powder diffraction (XRD) patterns of the samples were recorded on a Bruke D8 Advance powder X-ray diffractometer with Cu Kα (λ=0.15406 nm) over a range of 10-70° (*2θ*) with 0.02° per step. A HITACHI S-4800 field emission scanning electron microscope (FE-SEM) was used to characterize the morphologies of the synthesized samples. High resolution transmission electron microscopic (HRTEM) images were acquired with a JOEL JEM 2100 microscope. UV-Vis diffuse reflectance spectra (DRS) of the samples were recorded on a Schimadzu UV 2550 spectrophotometer with an integrating sphere attachment within the range of 200 to 800 nm and with $BaSO_4$ as the reflectance standard.

2.4. Photocatalytic activity measurements

The photocatalytic activity of the Ag_3PO_4/CeO_2 heterostructures was investigated by the photodegradation of Rhodamine B (RhB, 10 mg/L). Prior to the irradiation, the suspension containing 250 mL of RhB solution and 0.10 g catalysts was magnetically stirred in the dark for 30 min to establish adsorption-desorption equilibrium between the surface of the catalysts and the dye under ambient conditions. A 300 W mercury lamp with a maximum emission at 356 nm was used as the UV source, a 300 W Xe arc lamp as the visible light source where the UV components were filtered out during visible light photocatalysis. The distance between it and the photocatalyst was 50 cm. The light intensity reaching the samples was measured using a radiometer and was found to be approximately 35 W m^{-2} in the visible-light range. At varied irradiation time intervals, an aliquot of the mixed solution was collected and centrifuged, and the residual RhB concentration in the supernatant was analyzed by UV-vis spectroscopic measurements (Hitachi UV-3100)

3. Results and discussion

3.1. Morphology and structure characterization of catalyst

Figure 1 illustrates the XRD patterns of the obtained pure CeO_2 nanoparticles, Ag_3PO_4 and Ag_3PO_4/CeO_2 p-n heterojunctions. It is observed that all of the diffraction peaks shown in Figure 1a and b can be indexed to the cubic fluorite-type CeO_2 structure (JCPDS no. 43-1002) and body-centered cubic structure of Ag_3PO_4 (JCPDS no. 06-0505), respectively. The sharp diffraction peaks of both Ag_3PO_4 and CeO_2 indicate their good crystallinity. No traces of other phases are detected, confirming the high purity of the samples. The XRD pattern of the Ag_3PO_4/CeO_2 p-n heterojunctions (Figure 1c) clearly matches with the polycrystalline structures of Ag_3PO_4 (the peak without the triangle mark) and CeO_2 (the peak with

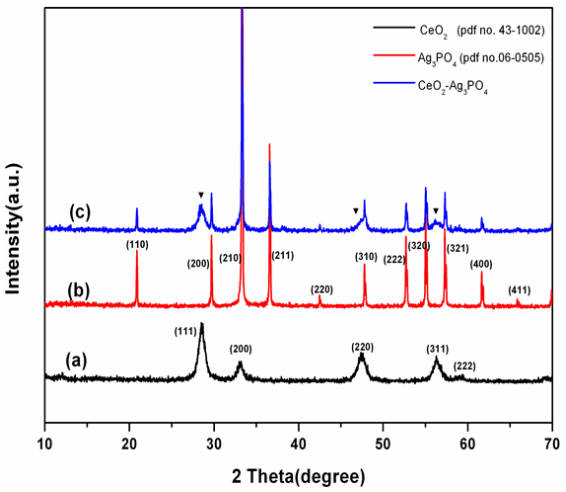

Figure 1 XRD patterns of (a) CeO2, (b) Ag3PO4 and (c) Ag3PO4/CeO2.

the triangle mark), indicating that the Ag_3PO_4/CeO_2 p-n heterojunctions has been successfully prepared.

The morphology of the as-synthesized pure CeO_2, Ag_3PO_4 and the Ag_3PO_4/CeO_2 p-n heterojunctions was examined by FE-SEM, as shown in Figure 2. It can be seen that pure CeO_2 (Figure 2a) exhibits spherical-shaped nanoparticls with diameters of about 30 nm, whereas pure Ag_3PO_4 is about 200-300 nm with a smooth surface (Figure 2b). When CeO_2 was deposited on the surface of Ag_3PO_4 *via* a facile precipitation-deposition process (Figure 2c-d), the resulting Ag_3PO_4/CeO_2 composite sample exhibits a similar morphology and size as compared to that of pure Ag_3PO_4. Obviously, the coexistence of CeO_2 and Ag_3PO_4 did not significantly affect their morphology. It is noticeable that the CeO_2 nanoparticls are uniformly distributed in the Ag_3PO_4 crystallites and form a composite structure. To further confirm the crystallographic structure of the Ag_3PO_4/CeO_2 p-n heterojunctions, high-resolution TEM (HRTEM) measurement was carried out (Figure 3). As shown

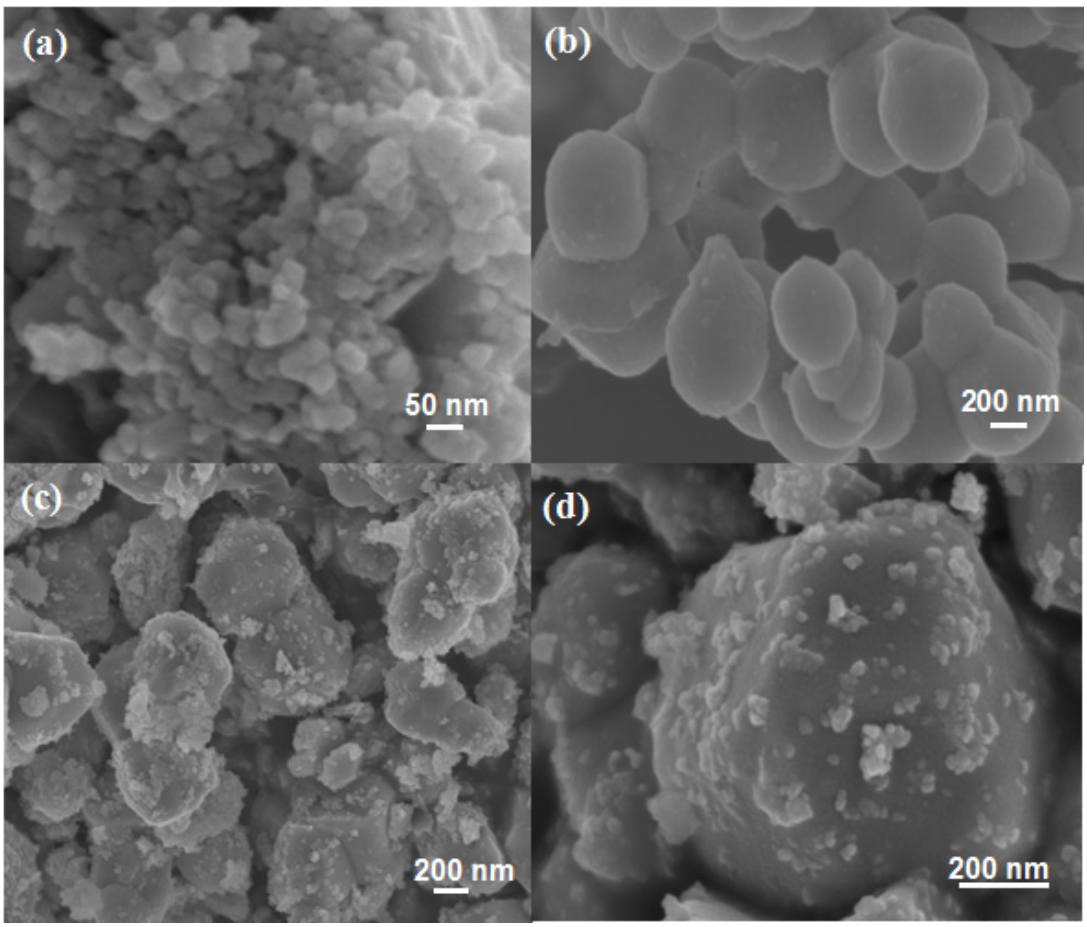

Figure 2 FE-SEM images of (a) CeO2, (b) Ag3PO4 and (c-d) Ag3PO4/ CeO2.

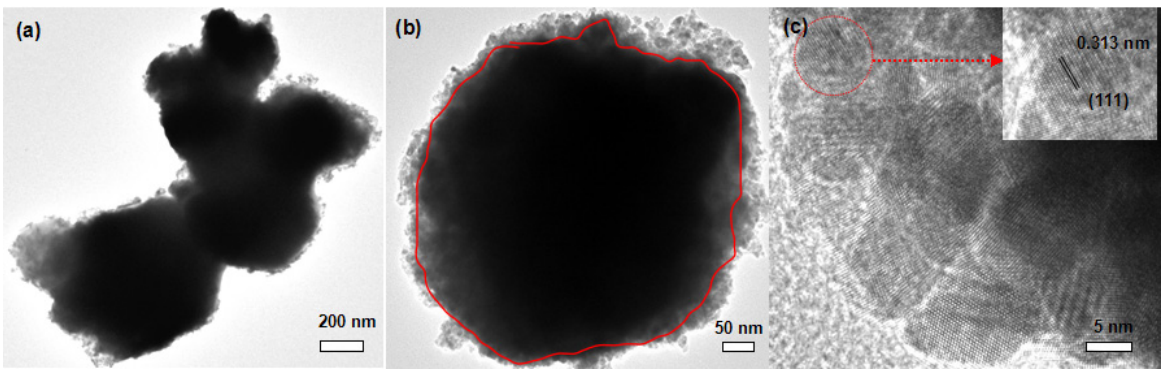

Figure 3 HRTEM images (a-c) of as prepared Ag3PO4/ CeO2 heterojunction.

in Figure 3b, the synthesized Ag_3PO_4/CeO_2 composite are of sphere morphology and is composed with inner Ag_3PO_4 core (Region I) and outer layer (Region II) of CeO_2 nanoparticle. Clear lattice fringes of the small CeO_2 nanocrystals can also be observed in Figure 3c, and inter-planar spacings are measured to be 0.313 nm, which agrees with the *d* values of the (111) plane of the cubic fluorite-type CeO_2.

3.2. UV-Vis absorption spectra

The optical absorption plays an important role in the photocatalysis, especially in the visible-light photodegradation of contaminants. The optical absorption properties of pure CeO_2, Ag_3PO_4 and the Ag_3PO_4/CeO_2 p-n heterojunctions were measured by UV-vis DRS and demonstrated in Figure 4. For pure CeO_2, an adsorption edge can be observed at 420 nm and can absorb solar energy with a wavelength shorter than 420 nm (Figure 4a), which is in agreement with the results previously reported [10, 11]. It can be clearly seen that pure yellow Ag_3PO_4 can absorb energy with wavelengths shorter than 550 nm (Figure 4b), in agreement with the results previously reported[15]. Upon the loading of the CeO_2 nanoparticles on the surface of Ag_3PO_4, the absorption edge of heterocrystals was drastically extended to around 560 nm and the absorption intensity in the region of 200-800 nm has been evidently increased. The red-shift of the absorption wavelength indicated that the photocatalyst could absorb more photons. Therefore, the red-shift in the absorption band could be favorable for photocatalytic reaction. These results clearly reveal that the *in situ* deposited of CeO_2 nanoparticles on the crystal surfaces of Ag_3PO_4 can serve as an effective strategy for enhancing their visible-light absorption.

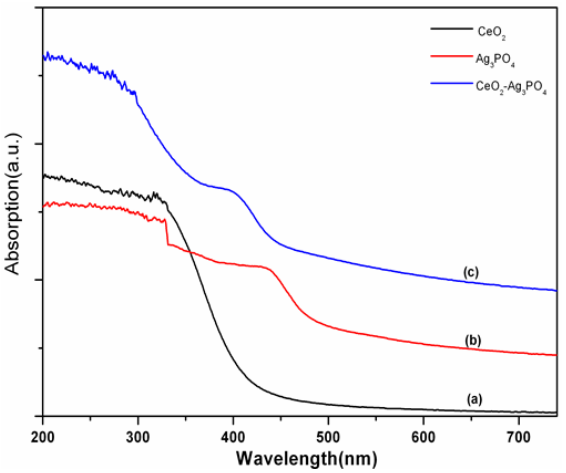

Figure 4 UV-vis absorption spectra of (a) CeO2, (b) Ag3PO4 and (c-d) Ag3PO4/ CeO2

3.3. Photocatalytic activity

3.3.1. Visible light photocatalytic activities of Ag_3PO_4/CeO_2

In this study, Rhodamine B (RhB), with a major absorption band at 554 nm, was chosen as a model pollutant for testing photocatalytic activity of the as-prepared products. The absorption spectra of RhB (Figure 5a), with 0.1 g of the Ag_3PO_4/CeO_2 p-n heterojunction photocatalyst under visible light irradiation, clearly show that the characteristic absorption peaks corresponding to RhB decrease rapidly as the exposure time increases, indicating the decomposition of RhB and the significant reduction in the RhB concentration. In this experiment, the photodegradation process is studied by monitoring the change in RhB concentration. The degradation efficiency of RhB over pure CeO_2, Ag_3PO_4 and the Ag_3PO_4/CeO_2 p-n heterojunctions under visible irradiation is presented in Figure 5b. It can be seen that 88.0% of the RhB is photocatalytically degraded after 60 min irradiation for the Ag_3PO_4/CeO_2 composite. For comparison, the activity of the Ag_3PO_4 photocatalyst was carried out under the same conditions. As shown in Figure 5b, the photocatalytic activity of the Ag_3PO_4 and CeO_2 sample for RhB degradation is much

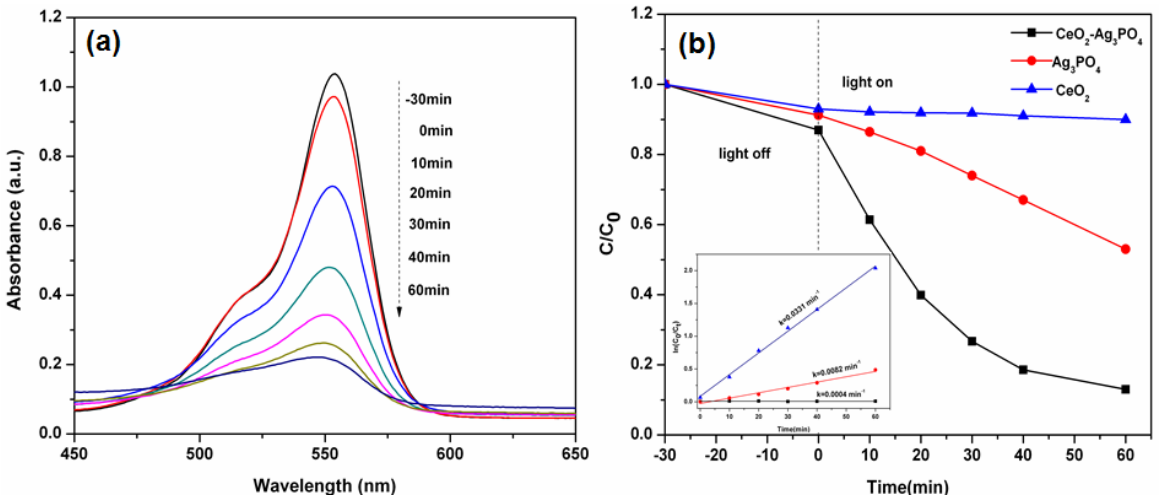

Figure 5 UV-vis absorbance spectra of RhB solution after photocatalytic degradation with Ag3PO4/ CeO2 heterojunction (a) and RhB concentration Ct/C0 and ln(C0/Ct) (inset)*vs.* time for the photocatalytic degradation of RhB with CeO_2, Ag_3PO_4 and Ag_3PO_4/CeO_2 (b) under visible light irradiation.

lower than that of the Ag_3PO_4/CeO_2 p-n heterojunctions. For the pure Ag_3PO_4 and CeO_2 samples, the RhB is degraded by only 47.0% and 10%, respectively.

To quantitatively investigate the reaction kinetics of the RhB degradation, the experimental data were fitted by a first-order model as expressed by the formula[13]:

$$-\ln(C/C_0) = kt$$

where C_0 and C are the dye concentrations in solution at times 0 and t, respectively, and k is the apparent first-order rate constant.

The kinetic data curves for RhB photocatalytic degradation with photocatalysts in the inset of Figure 5b show that the relationship between $\ln(C/C_0)$ and irradiation time is almost linear, suggesting that the photocatalytic reaction follows pseudo-first-order kinetics. As can be seen in Figure 5b, the pseudo-first-order rate constants (k) for RhB degradation with CeO_2, Ag_3PO_4 and Ag_3PO_4/CeO_2 composite were estimated to be 0.0004 min^{-1}, 0.0082 min^{-1}, 0.0331 min^{-1}, respectively. The rate constant of the Ag_3PO_4/CeO_2 composite is 82.8 times as high as that of CeO_2 and 4.0 times as that of Ag_3PO_4. The results demonstrate that the degradation efficiency of the Ag_3PO_4/CeO_2 composite to RhB in much higher than those of pure Ag_3PO_4 and CeO_2 under visible light irradiation. To elucidate the photocatalytic reaction mechanism, the main species including h^+, $\bullet O^{2-}$ and •OH involved in the photocatalytic process was examined. The method was applied according to the Xiang's report without any modifications[16]. The results indicated that h^+ and $\bullet O^{2-}$ were the main reactive oxidizing species in photocatalytic reaction process of Ag_3PO_4/Ag composites.

3.3.2. UV light photocatalytic activities of Ag_3PO_4/ CeO_2

Although CeO_2 has poor capacity for RhB degradation under visible light irradiation due to its higher band gap energy, it shows high photocatalytic capability in the UV region[17,18]. To investigate the effect of the coupling Ag_3PO_4 sensitizer on the photocatalytic capability of CeO_2, the photocatalytic degradation of RhB over CeO_2, Ag_3PO_4 and the Ag_3PO_4/CeO_2 p-n heterojunction under 300 W UV irradiation has also been performed. As shown in Figure 6, CeO_2 and Ag_3PO_4 show only 35% and 86% RhB degradation, whereas the Ag_3PO_4/CeO_2 composite renders 98.3% RhB degradation after 10 min of photocatalytic reaction. The Ag_3PO_4/CeO_2 composite exhibits the highest photocatalytic degradation efficiency, followed by the pure Ag_3PO_4 and CeO_2 photocatalysts. Additionally, pseudo-first-order rate constants (k) for RhB decomposition by the Ag_3PO_4/CeO_2 composite under UV light irradiation is about 0.2262 min^{-1}, faster than that with Ag_3PO_4 (0.0909 min^{-1}) and pure CeO_2 (0.0205 min^{-1}) by a factor of 2.5 and 11.0, respectively. The results demonstrate that the degradation efficiency of the Ag_3PO_4/CeO_2 composite to RhB in much higher than those of pure Ag_3PO_4 and CeO_2 under UV light irradiation.

3.3.3. photocatalytic stability

In addition to photocatalytic efficiency, the stability of photocatalyst is also very important for practical application. To evaluate the stability of the photocatalytic performance of Ag_3PO_4/CeO_2 composite, the circulating run in the photocatalytic degradation of RhB was carried out under visible light irradiation. As shown in Figure 7, the photocatalytic degradation efficiency of RhB still reached 82% after 3 cycles in 3 h. The decrease of degradation efficiency under the third run may be due to the loss of sample during the cycling reaction. Furthermore, the XRD analysis of Ag_3PO_4/CeO_2 photocatalyst before and after photocatalytic reaction indicated no difference between the two lines. The result demonstrates that the Ag_3PO_4/CeO_2 composite, formed by the coupling of CeO_2 and Ag_3PO_4, shows excellent photocatalytic performance, as well as good stability.

3.4. Photocatalytic mechanism of Ag_3PO_4/CeO_2 heterojunctions

Based on the above results, it is evident that the enhanced activity of the hybrid photocatalyst involving CeO_2 nanoparticles and Ag_3PO_4 can be attributed to the synergistic effects

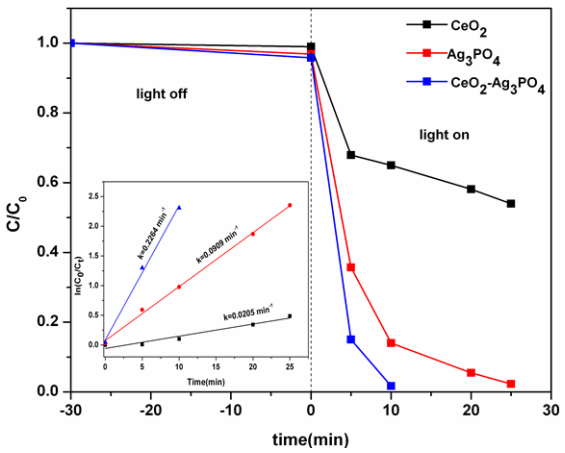

Figure 6 RhB concentration Ct/C0 and ln(C0/Ct) (inset)vs. time for the photocatalytic degradation of RhB with CeO_2, Ag_3PO_4 and Ag_3PO_4/ CeO_2 under UV light irradiation.

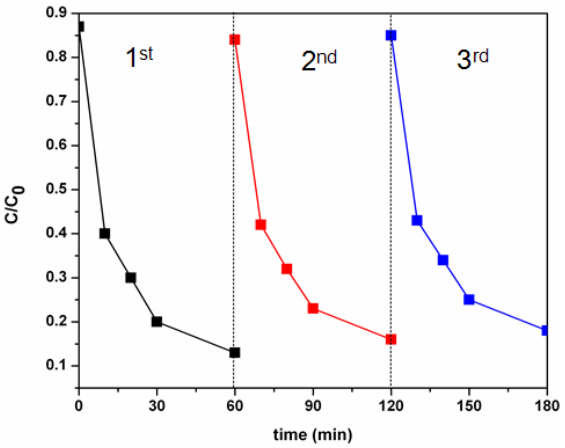

Figure 7 Cycling runs in the photocatalytic degradation of RhB with Ag3PO4/ CeO2 heterojunction under visible light irradiation.

of visible-light sensitization and p-n junction structure[19]. Ag_3PO_4 is a typical p-type semiconductor with a narrow band gap[15] while CeO_2 is an n-type semiconductor with a large band gap[20]. In order to fully understand the energy band structure of the p-Ag_3PO_4/n- CeO_2 heterojunction, the original energy band structures of Ag_3PO_4 and CeO_2 were provided. The valence band edge positions of Ag_3PO_4 and CeO_2 were estimated in this study according to the concept of electronegativity[18]. The conduction band (CB) and valence band (VB) positions of the two semiconductors at the point of zero charge are predicted theoretically by the following empirical equations[21]:

$$E_{VB} = X - E^e + 0.5\,E_g \quad (1)$$

$$E_{CB} = E_{VB} - E_g \quad (2')$$

where E_{CB} is the valence band (CB) potential; E_{VB} is the conduction band (VB) potential; X is the absolute electronegativity of the semiconductor, which is defined as the geometric mean of the absolute electronegativity of the constituent atoms; E^e is the energy of free electrons on the hydrogen scale (*ca.* 4.5 eV); and E_g is the band gap of the semiconductor. The conduction band (CB) position can be deduced by eqn (2). The X values for Ag_3PO_4 and CeO_2 are ca. 5.959 and 5.696 eV, respectively. The band-gap energies of Ag_3PO_4 and CeO_2, in our experiment, are estimated to be 2.32 and 2.86 eV, respectively. Herein, based on eqn (1) and (2), the top of the VB and the bottom of the CB for Ag_3PO_4 are calculated to be 2.619 and 0.299 eV respectively. Accordingly, the VB and CB of CeO_2 are estimated to be 2.626 and -0.234 eV, respectively. The energy band structure diagram of p-type Ag_3PO_4 and n-type CeO_2 is thus schematically illustrated in Figure 8a.

When p-type Ag_3PO_4 and n-type CeO_2 are in contact, The Fermi level of Ag_3PO_4 is raised up, while the Fermi level of CeO_2 is lowered until an equilibrium state is formed as shown in Figure 8b. Meanwhile, with the raising up and/or lowering of the Fermi level, the energy bands of Ag_3PO_4 shift upward along the Fermi level (E_{FP}) and those of the CeO_2 shift downward along its Fermi level (E_{Fn}), and as a result, the conduction band edge of p-type Ag_3PO_4 is higher than that of n-type CeO_2, leading to the formation of a p-n junction at the interface between Ag_3PO_4 and CeO_2 crystals. Thus, at the thermodynamic equilibrium, an inner electric field orienting from CeO_2 to Ag_3PO_4 was established in the interface between CeO_2 and Ag_3PO_4.

Therefore, we speculated a photocatalytic mechanism of the p-Ag_3PO_4/n-CeO_2 heterojunction as follows: under visible light illumination, Ag_3PO_4 acting as a photosensitizer could be easily activated by visible light and generated electrons and holes. From Figure 8b, it can be found that under the function of an internal electric field, the electrons from the excited Ag_3PO_4 transfer to the conduction band of CeO_2, and simultaneous holes remain in the p-Ag_3PO_4 valence band. In such a way, the photogenerated electron-hole pairs will be separated effectively by the p-n junction formed in the heterostructured p-Ag_3PO_4/n-CeO_2 interface and the photocatalytic activity is much enhanced. That is to say, to some extent, the recombination of photogenerated electrons and holes can be restrained. Furthermore, the migration rates of the photogenerated electrons and holes are promoted by the internal electric field in the p-n heterojunctions. The efficient charge separation could increase the lifetime of the charge carriers and has enough time to react with the reactants adsorbed onto the photocatalyst surfaces so as to improve the photocatalytic activity. According to the above results and discussion, it is apparent that the synergetic effects of the p-n junction formed between Ag_3PO_4 and CeO_2 were responsible for the enhanced visible-light photocatalytic activity.

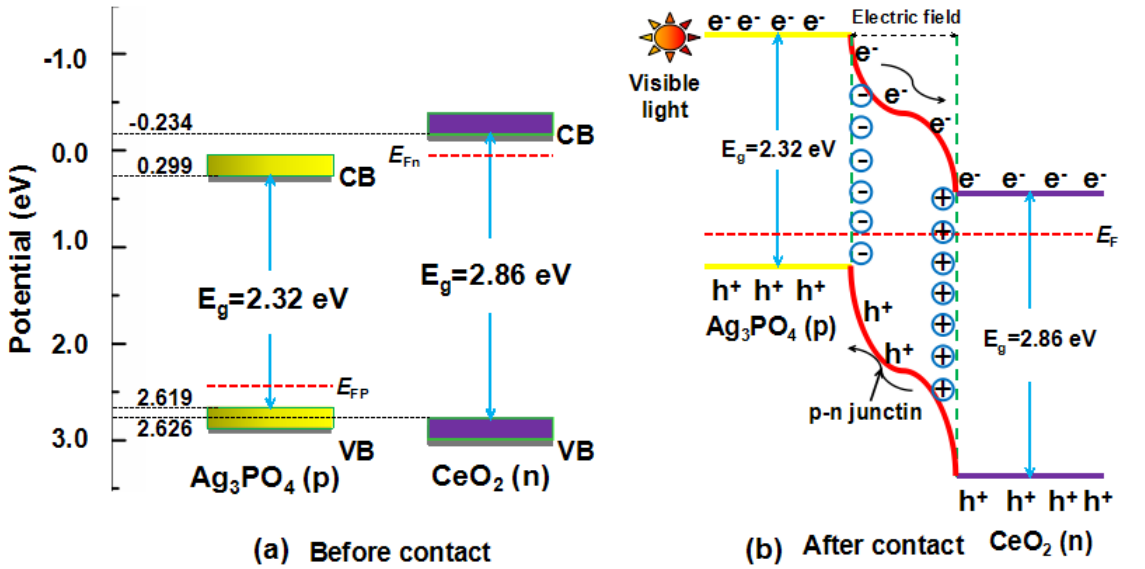

Figure 8 Schematic diagrams for (a) energy bands of p-Ag3PO4 and n-CeO2before contact and (b) the formation a p-n junction and its energy banddiagram at equilibrium and transfer of photoinduced electrons form p-Ag3PO4 and n-CeO2 under visible-light irradiation.

4. Conclusions

In summary, we have successfully fabricated Ag_3PO_4/CeO_2 p-n heterojunctions by depositing small CeO_2 nanoparticles sized of 10-15 nm on the surface of Ag_3PO_4 via a facile precipitation route. The obtained Ag_3PO_4/CeO_2 p-n heterojunctions exhibited enhanced photocalytic activity toward RhB degradation under ultra-violet and light irradiation than that of pure Ag_3PO_4 and CeO_2 nanoparticles. Such enhanced photocatalytic activity of the Ag_3PO_4/CeO_2 p-n heterojunctions could be attributed to high dispersibility of small CeO_2 nanoparticles, broadened of the optical absorption range as well as the generation of a p-n junction between p-type Ag_3PO_4 and n-type CeO_2. This work not only supports the possibility of using cost-effective n-type CeO_2 for photocatalytic degradation organic dye but also shows that a suitable p-n junction structure is crucial for high photocatalytic activity in a hybrid photocatalyst.

Acknowledgements

This research was financially supported by the Natural Science Foundation of AnHui Provincial Education Department (KJ2015A085) and National Undergraduate Training Programs for Innovation and Entrepreneurship

References

1. Sang Y, Liu H, Umar A. Photocatalysis from UV/Vis to near-infrared light: towards full solar-light spectrum activity. *ChemCatChem*. 2015;7:559-573. http://dx.doi.org/ 10.1002/cctc.201402812
2. Sang Y, Zhao Z, Zhao M, Hao P, Leng Y, Liu H. From UV to near-infrared, WS_2 nanosheet: a novel photocatalyst for full solar light spectrum photodegradation. *Advanced Materials*. 2015;27:363-369. http://dx.doi.org/10.1002/adma.201403264
3. Yi Z, Ye J, Kikugawa N, Kako T, Ouyang S, Stuart-Williams H, et al. An orthophosphate semiconductor with photooxidation properties under visible-light irradiation. *Nature Materials*. 2010;9:559-564. http://dx.doi.org/10.1038/nmat2780
4. Bi Y, Ouyang S, Umezawa N, Cao J, Ye J. Facet effect of single-crystalline Ag_3PO_4 sub-microcrystals on photocatalytic properties. *Journal of the American Chemical Society*. 2011;133:6490-6492. http://dx.doi.org/10.1021/ja2002132
5. Bi Y, Hu H, Ouyang S, Lu G, Cao J, Ye J. Photocatalytic and photoelectric properties of cubic Ag_3PO_4 sub-microcrystals with sharp corners and edges. *Chemical Communication*. 2012;48:3748-3750. http://dx.doi.org/10.1039/c2cc30363a
6. Wang H, Zhang L, Chen Z, Hu J, Li S, Wang Z, et al. Semiconductor heterojunction photocatalysts: design, construction, and photocatalytic performances. *Chemical Society Reviews*. 2014;43:5234-5244. http://dx.doi.org/10.1039/c4cs00126e
7. Lv Y, Huang K, Zhang W, Yang B, Chi F, Ran S et al. One step synthesis of $Ag/Ag_3PO_4/BiPO_4$ double-heterostructured nanocomposites with enhanced visible-light photocatalytic activity and stability. *Ceramics International*. 2014;40:8087-8092. http://dx.doi.org/10.1016/j.ceramint.2013.12.162
8. Wang W, Wang J, Wang Z, Wei X, Liu L, Ren Q, et al. p-n junction $CuO/BiVO_4$ heterogeneous nanostructures: synthesis and highly efficient visible-light photocatalytic performance. *Dalton Transactions*. 2014;43:6735-6743. http://dx.doi.org/10.1039/c3dt53613k
9. Wang T, Meng H, Yu X, Liu Y, Chen H, Zhu Y, et al. p-BiOI/n-SnS_2 heterojunction flowerlike structure with enhanced visible-light photocatalytic performance. *RSC Advances*. 2015;5:15469-15478. http://dx.doi.org/10.1039/c4ra15770b
10. Arul NS, Mangalaraj D, Ramachandran R, Grace AN, Han JI. Fabrication of CeO_2/Fe_2O_3 composite nanospindles for enhanced visible light driven photocatalysts and supercapacitor electrodes. *Journal of Materials Chemistry A*. 2015;3:15248-15258. http://dx.doi.org/10.1039/c5ta02630j
11. Wang Q, Yu S, Tan Z, Zhang R, Li Z, Gao X, et al. Synthesis of monodisperse Bi_2O_3-modified CeO_2 nanospheres with excellent photocatalytic activity under visible light. *CrystEngComm*. 2015;17:671-677. http://dx.doi.org/10.1039/c4ce02053g
12. Lu X-H, Xie S-L, Zhai T, Zhao Y-F, Zhang P, Zhang Y-L et al. Monodisperse CeO_2/CdS heterostructured spheres: one-pot synthesis and enhanced photocatalytic hydrogen activity. *RSC Advances*. 2011;1:1207-1210. http://dx.doi.org/10.1039/c1ra00252j
13. Huang L, Li Y, Xu H, Xu Y, Xia J, Wang K, et al. Synthesis and characterization of CeO_2/g-C_3N_4 composites with enhanced visible-light photocatatalytic activity. *RSC Advances*. 2013;3:22269-22279. http://dx.doi.org/10.1039/c3ra42712a
14. Yang ZM, Huang GF, Huang WQ, Wei JM, Yan XG, Liu YY, et al. Novel Ag_3PO_4/CeO_2 composite with high efficiency and stability for photocatalytic applications. *Journal of Materials Chemistry A*. 2014;2:1750-1756. http://dx.doi.org/10.1039/c3ta14286h
15. Lin H, Ye H, Xu B, Cao J, Chen S. Ag_3PO_4 quantum dot sensitized $BiPO_4$: a novel p-n junction $Ag_3PO_4/BiPO_4$ with enhanced visible-light photocatalytic activity. *Catalysis Communications*. 2013;37:55-59. http://dx.doi.org/10.1016/j.catcom.2013.03.026
16. Xiang QJ, Lang D, Shen TT, Liu F. Graphene-modified nanosized Ag_3PO_4 photocatalysts for enhanced visible-light photocatalytic activity and stability. *Applied Catalysis B: Environmental*. 2015;162:196-203. http://dx.doi.org/10.1016/j.apcatb.2014.06.051
17. Song S, Xu L, He Z, Ying H, Chen J, Xiao X et al. Photocatalytic degradation of C.I. Direct Red 23 in aqueous solutions under UV irradiation using $SrTiO_3/CeO_2$ composite as the catalyst. *Journal of Hazardous materials*. 2008;152:1301-1308. http://dx.doi.org/10.1016/j.jhazmat.2007.08.004
18. Lu X, Zhai T, Cui H, Shi J, Xie S, Huang Y, et al. Redox cycles promoting photocatalytic hydrogen evolution of CeO_2 nanorods. *Journal of Materials Chemistry*. 2011;21:5569-5572. http://dx.doi.org/10.1039/c0jm04466k
19. Dai G, Yu J, Liu G. Synthesis and enhanced visible-Light photoelectrocatalytic activity of p–n junction $BiOI/TiO_2$ nanotube Arrays. *The Journal of Physical Chemistry C*. 2011;115:7339-7346. http://dx.doi.org/10.1021/jp200788n
20. Yang ZM, Hou SC, Huang GF, Duan HG, Huang WQ. Electrospinning preparation of p-type NiO/n-type CeO_2 heterojunctions with enhanced photocatalytic activity. *Materials Letters*. 2014;133:109-112. http://dx.doi.org/10.1016/j.matlet.2014.06.169
21. Jiang D, Chen L, Zhu J, Chen M, Shi W, Xie J. Novel p-n heterojunction photocatalyst constructed by porous graphite-like C_3N_4 and nanostructured BiOI: facile synthesis and enhanced photocatalytic activity. *Dalton Transactions*. 2013;42:15726-15734. http://dx.doi.org/10.1039/c3dt52008k